SpezialForschungsBereich F 32

Karl–Franzens Universität Graz
Technische Universität Graz
Medizinische Universität Graz

Comparison of the Reduced-Basis and POD a-Posteriori Error Estimators for an Elliptic Linear-Quadratic Optimal Control

T. Tonn K. Urban S. Volkwein

SFB-Report No. 2010–013 April 2010

A–8010 GRAZ, HEINRICHSTRASSE 36, AUSTRIA

Supported by the
Austrian Science Fund (FWF)

SFB sponsors:

- **Austrian Science Fund** (FWF)
- **University of Graz**
- **Graz University of Technology**
- **Medical University of Graz**
- **Government of Styria**
- **City of Graz**

Mathematical and Computer Modelling of Dynamical Systems
Vol. 00, No. 00, March 2010, 1–13

Article

Comparison of the Reduced-Basis and POD a-Posteriori Error Estimators for an Elliptic Linear-Quadratic Optimal Control Problem

Timo Tonn[a], K. Urban[a] and S. Volkwein[b*]

[a]*Institut für Numerische Mathematik, Universität Ulm, Helmholtzstrasse 18, D-89069 Ulm, Germany*; [b]*Fachbereich Mathematik und Statistik, Universität Konstanz, Universitätsstraße 10, D-78457 Konstanz, Germany*

(*February 2010*)

In this article, a linear-quadratic optimal control problem governed by the Helmholtz equation is considered. For the computation of suboptimal solutions, two different model reduction techniques are compared: the reduced-basis method (RBM) and proper orthogonal decomposition (POD). By an a-posteriori error estimator for the optimal control problem the accuracy of the suboptimal solutions is ensured. The efficiency of both model reduction approaches is illustrated by a numerical example.

Keywords: optimal control, a-posteriori error estimate, proper orthogonal decomposition, reduced-basis method

AMS Subject Classification: 49K20, 65K10, 90C20, 90C46

1. Introduction

Optimal control problems for partial differential equations are often hard to tackle numerically because their discretization leads to very large scale optimization problems. Therefore, different techniques of model reduction have been developed to approximate these problems by smaller ones that are tractable with less effort. Among them, the reduced-basis (RB) and the proper orthogonal decomposition (POD) method are widely used, also in the context of nonlinear problems.

Some reduced order methods like balanced truncation offer a reliable a-priori error analysis for optimal control applications, [1, 2]. However, for POD and RB it is not a-priori clear how far the optimal control of the reduced-order problem is from the exact one, unless its snapshots are generating a sufficiently rich space, where sufficiently rich implies that the space contains all possible snapshots. However, we are able to compensate for the lack of a-priori analysis for the POD and RB method by utilizing an a-posteriori analysis. This approach is based on a fairly standard perturbation argument to deduce how far the suboptimal control, computed on the basis of the reduced-order method, is away from the (unknown) exact one.

*Corresponding author. Email: Stefan.Volkwein@uni-konstanz.de

ISSN: 1387-3954 print/ISSN 1744-5051 online

DOI: 10.1080/1387395YYxxxxxxxx
http://www.informaworld.com

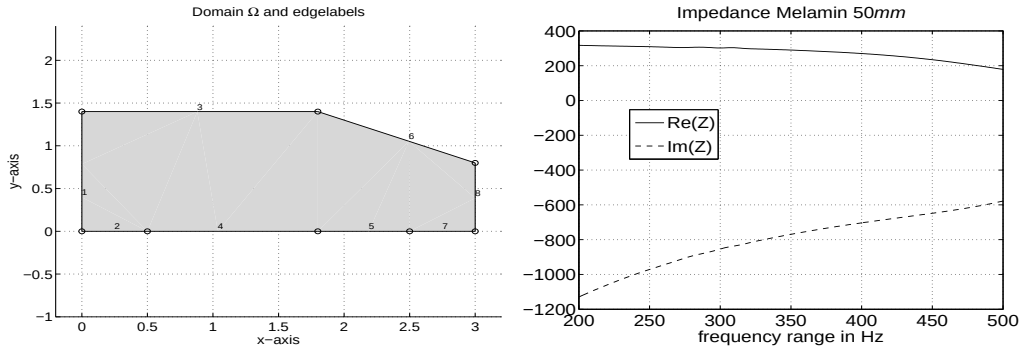

(a) (b)

Figure 1. Two-dimensional cross section of an idealized interior Ω of the vehicle, where the boundary part Γ_R consists of parts 4 and 5 (a); impedance values $Z = Z_{\Re} + \jmath Z_{\Im}$ for melamine 50mm width in the frequency range from 200 to 500 Hz (b).

2. The optimal control problem and optimality conditions

In this section, we introduce the linear-quadratic elliptic optimal control problem, recall the associated first-order necessary optimality conditions and define a reduced problem only for the control variable.

The optimal control problem

Suppose that the interior of a car is simplified by the two-dimensional domain Ω plotted in Figure 1 (a). The boundary $\Gamma = \partial\Omega$ is split into two measurable disjunct parts Γ_R and Γ_N.

Denoting the frequency by f, let $0 \neq Z_f \in \mathbb{C}$ (see Figure 1 (b)) be a given complex impedance. Then, the associated sound pressure $p : \Omega \to \mathbb{C}$ is governed by the Helmholtz equation

$$-\Delta p(\mathbf{x}) - k_f^2\, p(\mathbf{x}) = u\, b(\mathbf{x}) \quad \text{for all } \mathbf{x} = (x_1, x_2) \in \Omega, \tag{1a}$$

together with the boundary conditions

$$\frac{\jmath}{\varrho_\circ\, \omega_f} \frac{\partial p(\mathbf{x})}{\partial n} = \frac{p(\mathbf{x})}{Z_f} \qquad \text{for all } \mathbf{x} \in \Gamma_R, \tag{1b}$$

$$\frac{\jmath}{\varrho_\circ\, \omega_f} \frac{\partial p(\mathbf{x})}{\partial n} = 0 \qquad \text{for all } \mathbf{x} \in \Gamma_N. \tag{1c}$$

In (1), $\varrho_\circ = 1.19985\big[\frac{kg}{m^3}\big]$ is an ambient density, $\omega_f = 2\pi f$ is the circle frequency and $k_f = \omega_f / c$ is the wave number, where the constant $c = 343.799\big[\frac{m}{s}\big]$ denotes the speed of sound. The right-hand side is a simplified model for a source at the point $\mathbf{x}_q = (0.21, 1.28)$ (e.g., a loudspeaker located at $\mathbf{x}_q$) with the intensity $|u|$, $u \in \mathbb{C}$, and shape function

$$b(\mathbf{x}) = \exp(-50\left(\|\mathbf{x} - \mathbf{x}_q\|_2^2\right) \quad \text{for } \mathbf{x} = (x_1, x_2) \in \Omega.$$

For the normal impedance boundary condition (1b), let $\jmath$ be the imaginary unit and $\frac{\partial}{\partial n}$ denote the derivative in the outward normal direction. All other parts on the boundary are assumed to be perfectly rigid, see (1c). Throughout the paper, we suppose the following assumption.

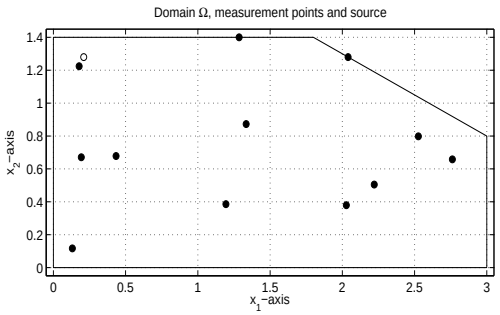

Figure 2. Measurement points (•) and location of the source (∘) for our numerical examples.

Assumption 1: For all given frequencies $f \in \mathcal{F} := [200\,\mathrm{Hz}, 500\,\mathrm{Hz}]$, all given $u \in \mathbb{C}$ and the impedance function Z_f, plotted in Figure 1 (b), the problem (1) admits a unique solution $p = p_f(u)$.

Remark 1 : Due to the Fredholm theory, [3], we can ensure existence of a solution provided k_f^2 is not an eigenvalue of $-\Delta$ considered on Ω with Neumann and Robin boundary conditions on Γ_N and Γ_R, respectively. □

Let $p_f^i \in \mathbb{C}$, $i = 1, \ldots, n_\mathrm{m}$, $n_\mathrm{m} \in \mathbb{N}$, be measured sound pressures at different given observation points $\mathbf{x}_i \in \Omega \cup \Gamma_N$, $1 \le i \le n_\mathrm{m}$; see Figure 2 for given frequency $f \in \mathcal{F}$. We introduce the quadratic cost functional

$$J_f(p,u) := \frac{\alpha}{2} \sum_{i=1}^{n_\mathrm{m}} \left| p(\mathbf{x}_i) - p_f^i \right|^2 + \frac{\sigma}{2} \left| u - u_f^\circ \right|^2,$$

where $u_f^\circ \in \mathbb{C}$ is a given reference intensity, $|z|$ is the absolute modulus of a complex number z, α is non-negative and σ is positive. Then, given f, we consider the optimal control problem

$$\min J_f(x_f) \quad \text{subject to (s.t.)} \quad x_f = (p_f, u_f) \text{ solves (1).} \qquad (\mathbf{P}_f)$$

Thus, $(\mathbf{P}_f)$ is a linear-quadratic optimal control problem for any frequency $f \in \mathcal{F}$.

First-order optimality conditions

The first-order necessary optimality conditions to $(\mathbf{P}_f)$ consist of the state equation, the adjoint system for the Lagrange multiplier λ_f^*

$$\begin{aligned}
-\Delta \lambda_f^*(\mathbf{x}) - k_f^2 \lambda_f^*(\mathbf{x}) &= \alpha \sum_{i=1}^{n_\mathrm{m}} (p_f^i - p_f^*(\mathbf{x}_i)) \delta_{\mathbf{x}_i}(\mathbf{x}) && \text{for all } \mathbf{x} \in \Omega, \\
\frac{\jmath}{\varrho_\circ \, \omega_f} \frac{\partial \lambda_f^*(\mathbf{x})}{\partial n} &= -\frac{\lambda_f^*(\mathbf{x})}{\overline{Z}_f} && \text{for all } \mathbf{x} \in \Gamma_R, \\
\frac{\jmath}{\varrho_\circ \, \omega_f} \frac{\partial \lambda_f^*(\mathbf{x})}{\partial n} &= 0 && \text{for all } \mathbf{x} \in \Gamma_N
\end{aligned}$$

and the equation for the optimal control u_f^*

$$\sigma\big(u_f^* - u_f^\circ\big) - \int_\Omega b(\mathbf{x})\lambda^*(\mathbf{x})\,\mathrm{d}\mathbf{x} = 0 \quad \text{in } \mathbb{C},$$

where $\delta_{\mathbf{x}_i}$ denotes the Dirac delta distribution satisfying

$$\langle \delta_{\mathbf{x}_i}, \varphi\rangle = \varphi(\mathbf{x}_i) \quad \text{for } \varphi \in C(\Omega \cup \Gamma_N) \text{ and } i = 1, \ldots, n_{\mathrm{m}}.$$

As usual $\overline{z} = x - \jmath y$ is the complex conjugate of $z = x + \jmath y \in \mathbb{C}$. For more details we refer the reader to [4, 5].

The reduced problem

Motivated by Assumption 1 we introduce the reduced cost functional $\hat{J} : \mathbb{C} \to [0, \infty)$ by

$$\hat{J}_f(u) = J_f(p_f(u), u) \quad \text{for } u \in \mathbb{C}$$

where $p_f(u)$ again denotes the unique solution to (1) for a given control input u at a given frequency f. Then, $(\mathbf{P}_f)$ is equivalent to the reduced optimal control problem

$$\min \hat{J}_f(u_f) \quad \text{s.t.} \quad u_f \in \mathbb{C}. \tag{$\hat{\mathbf{P}}_f$}$$

If $x_f^* = (p_f^*, u_f^*)$ is an optimal solution to $(\mathbf{P}_f)$, then u_f^* solves $(\hat{\mathbf{P}}_f)$. On the other hand, if u_f^* is an optimal solution to $(\hat{\mathbf{P}}_f)$, then the pair $(p_f(u_f^*), u_f^*)$ solves $(\mathbf{P}_f)$. The ultimate goal is to determine the optimal control for many values $f \in \mathcal{F}$. In order to avoid a naive and possibly costly evaluation of the elliptic linear-quadratic optimal control problem for various values of f we introduce a model reduction. This leads to a reduced-order model for $(\hat{\mathbf{P}}_f)$. The accuracy of the reduced-order model is controlled by an a-posteriori error analysis. This is the focus of the next section.

3. A-posteriori error estimate for the optimal control problem

In this section we recall some results of the a-posteriori error estimator. For more details, we refer the reader to [6, 7]. Suppose that $u \in \mathbb{C}$ is an arbitrary control input. Then, the difference $|u_f^* - u|$ can be estimated without requiring knowledge of u_f^*.

Theorem 3.1: *Let u_f^* be an optimal solution to $(\hat{\mathbf{P}}_f)$. Let p_f^* and λ_f^* be the associated state variable and Lagrange multiplier, respectively. Suppose that $u \in \mathbb{C}$*

is chosen arbitrarily, $p_f = p_f(u)$ *solves* (1) *and* $\lambda_f = \lambda_f(p_f)$ *solves*

$$\begin{aligned} \Delta\lambda_f(\mathbf{x}) + k_f^2\lambda_f(\mathbf{x}) &= \alpha\sum_{i=1}^{n_{\mathrm{m}}}(p_f^i - p_f(\mathbf{x}_i))\delta_{\mathbf{x}_i}(\mathbf{x}), \quad \textit{for all } \mathbf{x}\in\Omega, \\ \frac{\jmath}{\varrho_\circ\,\omega_f}\frac{\partial\lambda_f(\mathbf{x})}{\partial n} &= -\frac{\lambda_f(\mathbf{x})}{\overline{Z}_f}, \qquad\qquad \textit{for all } \mathbf{x}\in\Gamma_R, \\ \frac{\jmath}{\varrho_\circ\,\omega_f}\frac{\partial\lambda_f(\mathbf{x})}{\partial n} &= 0, \qquad\qquad \textit{for all } \mathbf{x}\in\Gamma_N. \end{aligned} \tag{2}$$

Then, it follows that

$$\left|u_f^* - u\right| \le \frac{1}{\sigma}\left|\zeta_f\right|, \tag{3}$$

where $\zeta_f = \zeta_f(u,\lambda_f) = \sigma\big(u - u_f^\circ\big) - \int_\Omega b(\mathbf{x})\lambda_f(\mathbf{x})\,\mathrm{d}\mathbf{x}$.

Proof: The claim follows from Theorem 3.1, Proposition 3.2, and Remark 3.3 in [6]. □

We will call the right-hand side of (3) an a-posteriori error estimate, since, in the next two sections, we shall apply it to suboptimal controls $u = \hat{u}_f$ that have been computed from a reduced-order model (utilizing the reduced-basis respectively the POD method). After having computed $\hat{u}_f$, we determine the associated state $\hat{p}_f = p_f(\hat{u}_f)$ and adjoint state $\hat{\lambda}_f = \lambda_f(\hat{p}_f)$. Then, we can compute $\hat{\zeta}_f = \zeta_f(\hat{u}_f, \hat{\lambda}_f)$ and its norm, s.t. (3) gives an upper bound for the distance of $\hat{u}_f$ to u_f^*. In this way, the error $|u_f^* - \hat{u}_f|$ caused by the reduced-order model can be estimated a-posteriori. If the error is too large, we have to include more basis functions into the reduced model.

4. Reduced-order methods

In this section, we introduce the reduced-order modeling for (1) utilizing POD and RBM. Let us emphasize that the computation of the reduced-order model is only based on the state equation (1), so that no information from the optimal solution of $(\mathbf{P}_f)$ is needed.

4.1. *Proper orthogonal decomposition*

In this subsection, we briefly review the POD method for our problem and derive the reduced-order model. Let X be either the Lebesgue space $L_2(\Omega)$ supplied with the inner product

$$\langle\psi,\varphi\rangle_{L_2(\Omega)} = \int_\Omega \psi\varphi\,\mathrm{d}\mathbf{x} \quad \text{for } \psi,\varphi\in L_2(\Omega)$$

or the Sobolev space $H^1(\Omega)$ endowed with the common inner product

$$\langle\psi,\varphi\rangle_{H^1(\Omega)} = \int_\Omega (\nabla\psi\cdot\nabla\varphi + \psi\varphi)\,\mathrm{d}\mathbf{x} \quad \text{for } \psi,\varphi\in H^1(\Omega).$$

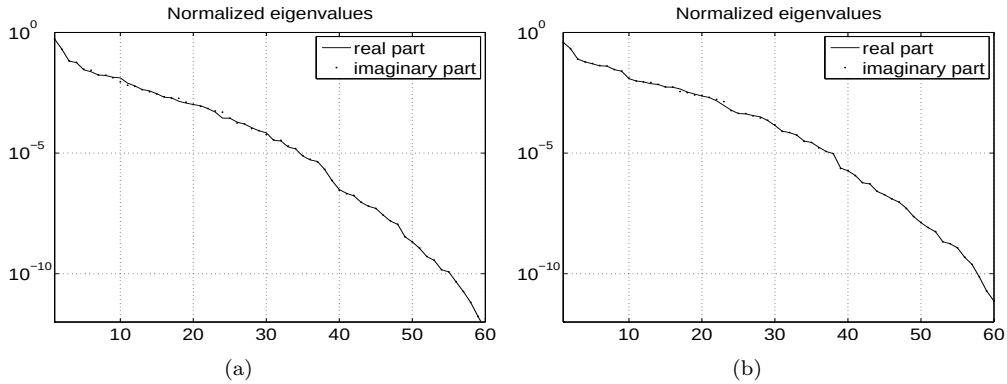

(a) (b)

Figure 3. Decay of the first 60 POD eigenvalues for $X = L_2(\Omega)$ (a) and $X = H^1(\Omega)$ (b).

Note that (1) is a linear elliptic equation and u is a complex number. Thus, by linear superposition for any frequency f, the solution to (1) is given by a linear combination of p_1 and p_2, where p_1 solves (1) for $u = 1$ and p_2 is the solution to (1) for $u = \jmath$.

Let $\Xi_f := \{f_1, \ldots, f_n\} \subset \mathcal{F}$ be a given snapshot grid. We denote by $p_j = \Re(p_1(f_j))$ and $p_{j+n} = \Re(p_2(f_j))$[1] the real part of the solution p to (1) for $u = 1$ and $u = \jmath$, respectively, at frequency instances f_j, $j = 1, \ldots, n$. Let $V_\Re = \operatorname{span}\{p_1, \ldots, p_{2n}\} \subset X$ with $d^\Re := \dim V_\Re \leq 2n$. Then, for given $\ell \leq 2n$ we consider the minimization problem

$$\begin{cases} \min\limits_{\psi_1,\ldots,\psi_\ell \in X} \sum\limits_{j=1}^{2n} \left\| p_j - \sum\limits_{i=1}^{\ell} \langle p_j, \psi_i \rangle_X \, \psi_i \right\|_X^2 \\ \quad \text{s.t.} \quad \langle \psi_i, \psi_j \rangle_X = \delta_{ij} \text{ for } 1 \leq i, j \leq \ell. \end{cases} \tag{4}$$

Remark 1: In some applications, the mean value of the snapshots is included in the POD modeling (see, e.g., in [8]). In our numerical experiments it turns out that this approach does not give rise to better results.

The solution to (4) is given by the solution of the eigenvalue problem

$$\mathcal{R}\psi_i = \sum_{j=1}^{2n} \langle p_j, \psi_i \rangle_X \, p_j = \lambda_i \psi_i \quad \text{for } i = 1, \ldots, \ell,$$

where $\mathcal{R} : X \to V_\Re \subset X$ is a linear, bounded, compact, self-adjoint and non-negative operator; see [8]. Thus, there exists an orthonormal set $\{\psi_i\}_{i=1}^{d^\Re}$ of eigenfunctions and corresponding non-negative eigenvalues $\{\lambda_i\}_{i=1}^{d^\Re}$ satisfying

$$\mathcal{R}\psi_i = \lambda_i \psi_i, \quad \lambda_1 \geq \lambda_2 \geq \cdots \geq \lambda_{d^\Re} \geq 0.$$

In [9] the dependence of $\{\psi_i\}_{i=1}^{\ell}$ and $\{\lambda_i\}_{i=1}^{\ell}$ for $\ell \leq 2n$ on the chosen snapshot grid $\{f_j\}_{j=1}^{n}$ is investigated.

Analogously, a POD basis $\{\phi_i\}_{i=1}^{\ell}$ for the snapshot space $V_\Im = \operatorname{span}\{\Im(p_{1,1}), \ldots, \Im(p_{1,n}), \Im(p_{2,1}), \ldots, \Im(p_{2,n})\} \subset X$ can be introduced. Since the eigenvalues for the real and for the imaginary parts decay in a similar rate (see

[1]For $z = x + \jmath y \in \mathbb{C}$ we use the notation $\Re(z) := x$ and $\Im(z) := y$.

Figure 3), we choose the same number of ansatz functions for the real and for the imaginary parts. In order to highlight similarities and differences of POD and RB method we stress, that the modes are linear combinations of *all* snapshots p_j, $j = 1, \dots, n$.

4.2. *The reduced-basis method*

Before going into detail on the application of the reduced basis method, we reconsider the snapshot generation of the POD from above. Recall that Ξ_f denotes the frequency snapshot grid which we now extend by the control, i.e. we introduce $\tilde{f} = (f, u) \in \mathcal{F} \times \mathbb{C}$ and $\Xi_{\tilde{f}} := \{\tilde{f} = (f, u) : f \in \Xi_f, u \in \{1, \jmath\}\}$. Then, for POD the snapshots are the solutions $p_{\tilde{f}} = p_f(u)$ of (1) for all $\tilde{f} \in \Xi_{\tilde{f}}$. In contrast to this, for the RBM, the Helmholtz equation (1) has to be solved for only some particular values in $\Xi_{\tilde{f}}$, where the selection procedure is stated below. As a start, let $S^\ell_{\tilde{f}} := \{\tilde{f}^*_1, \dots, \tilde{f}^*_\ell\} \subset \Xi_{\tilde{f}}$ denote the set of identified values, $V^\ell_\Re := \operatorname{span}\{\psi_i := \Re(p_{\tilde{f}^*_i}), 1 \le i \le \ell\} \subset X$ and $V^\ell_\Im := \operatorname{span}\{\phi_i := \Im(p_{\tilde{f}^*_i}), 1 \le i \le \ell\} \subset X$. Note, that for algebraic stability of the reduced order model, the bases $\{\psi_i\}^\ell_{i=1}$ and $\{\phi_i\}^\ell_{i=1}$ are orthonormalized w.r.t. $\|\cdot\|_X$ by a Gram-Schmidt procedure. Moreover, the modes are a linear combination of just a few snapshots.

Next, in order to identify frequencies in $S^\ell_{\tilde{f}}$, which lead to "good" resulting bases $\{\psi_i\}^\ell_{i=1}$ and $\{\phi_i\}^\ell_{i=1}$, we utilize the standard greedy procedure (c.p. [10]) using an a-posteriori error estimator $\Delta^\ell_{\tilde{f}}$ to be explained later, which reads:

Algorithm 1:

Set $\ell^{\max} \in \mathbb{N}$, $\varepsilon > 0$ and choose $\tilde{f}^*_1 \in \Xi_{\tilde{f}}$ arbitrarily.
for $l = 1$ **to** $\ell^{\max}$ **do**
  Compute $\varepsilon^\ell := \max_{\tilde{f} \in \Xi_{\tilde{f}}} \Delta^\ell_{\tilde{f}} / \|\hat{p}^\ell_{\tilde{f}}\|_{\mathcal{X}}$.
  if $\varepsilon^\ell < \varepsilon$ **or** $\ell = \ell^{\max}$ **then**
    break.
  else
    Set $\tilde{f}^*_{\ell+1} := \arg\max_{\tilde{f} \in \Xi_{\tilde{f}}} \Delta^\ell_{\tilde{f}} / \|\hat{p}^\ell_{\tilde{f}}\|_{\mathcal{X}}$.
    Compute $p_{\tilde{f}^*_{\ell+1}}$.
    Set $V^{\ell+1}_\Re = V^\ell_\Re \oplus \{\Re(p_{\tilde{f}^*_{\ell+1}})\}$ and $V^{\ell+1}_\Im = V^\ell_\Im \oplus \{\Im(p_{\tilde{f}^*_{\ell+1}})\}$.
  end if
end for

Note, that $\hat{p}^\ell_{\tilde{f}}$ in Algorithm **1** denotes the reduced order solution of (1) using $V^\ell_\Re \oplus \jmath V^\ell_\Im$ as trial- and testspaces. It is well known, that

$$\Delta^\ell_{\tilde{f}} := \frac{1}{\beta_{\tilde{f}}} \|R^\ell_{\tilde{f}}\|_{\mathcal{X}'}. \tag{5}$$

is a rigorous a-posteriori error estimator for $\|p_{\tilde{f}} - \hat{p}^\ell_{\tilde{f}}\|_{\mathcal{X}}$, where $\|\cdot\|_{\mathcal{X}} := \|\Re(\cdot)\|_X + \|\Im(\cdot)\|_X$, $\beta(f)$ is the *inf-sup constant* of (1) and $R^\ell_{\tilde{f}}$ is the residual of (1) for the reduced order solution $\hat{p}^\ell_{\tilde{f}}$.

Obviously, for the application in Algorithm **1**, $\Delta^\ell_{\tilde{f}}$ should be rapidly evaluable.

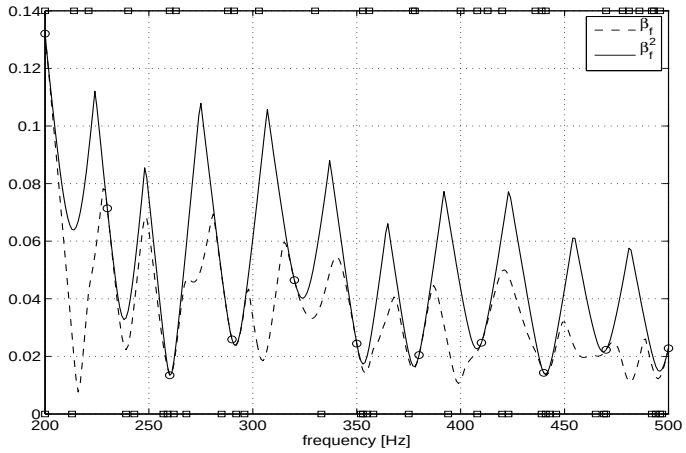

Figure 4. Inf-sup constant β_f its approximation $\hat{\beta}_f^2$ as well as $\tilde{f}_i^*$ identified by Algorithm **1**.

While this holds for the dual norm of the residual, which can be evaluated in $\mathcal{O}(\ell^2)$ (c.p. [10]), the evaluation of β_f is more involved than solving the actual problem (1). A possible way out is the application of the so called *Successive Constraint Method* (SCM, c.p. [11]) to obtain a *lower* bound to β_f that is rapidly evaluable, but at the cost of an expensive (offline) precomputation. On the other hand, in this work, we are interested in $\hat{u}_f^\ell$, the suboptimal solution to $(\hat{\mathbf{P}}_f)$, for which we already have an a-posteriori error estimator (c.p. Theorem 3.1), s.t. $\Delta_{\tilde{f}}^\ell$ does not necessarily need to be rigorous, rather than a good indicator.

Hence, the easiest way to avoid the cost of an expensive (offline) precomputation is to use $\hat{\beta}_f^1 = 1$. Another possibility is to compute β_f for some frequencies (say n), only, and use the part of the SCM that determines $\hat{\beta}_f^2$, an *upper* bound to β_f, in $\mathcal{O}(n)$. Figure 4 visualizes β_f as well as $\hat{\beta}_f^2$ obtained from computing β_f for equidistant f_i, $1 \leq i \leq n = 11$. Moreover, it shows the by Algorithm **1** identified values $\tilde{f}_i^* = (f_i^*, u_i^*)$, where f_i^* is marked on the bottom (top) axis if $u_i^* = 1$ ($u_i^* = 2$). We will investigate the differences resulting from using $\hat{\beta}_f^1 = 1$ and $\hat{\beta}_f^1 = 2$ as approximations to β_f in Section 5. The CPU time needed for computing $\hat{\beta}_f^2$ is reported in Table 1.

Remark 2: Note, that for the POD method the bases $\{\psi_i\}_{i=1}^\ell$ and $\{\phi_i\}_{i=1}^\ell$ are computed, s.t. the *mean* error to the snapshots is minimized (c.p. (4)), whereas for the RBM $\{\psi_i\}_{i=1}^\ell$ and $\{\phi_i\}_{i=1}^\ell$ are computed, s.t. the *maximum* error to the snapshots is minimized (c.p. Algorithm **1**).

The a-posteriori error estimator for $(\hat{\mathbf{P}}_f)$

The a-posteriori error estimator for $(\hat{\mathbf{P}}_f)$ is formulated in Algorithm **2**.

Algorithm 2:

Choose $\ell = 2$, $\ell^{\max} = 60$, and ε. Set flag $= 0$.
for $f = 200$ **to** 500 **do**

  repeat
    Set $\ell = \max(2, \ell - 2)$.
    Calculate the suboptimal solution $\hat{u}_f^\ell$ to $(\hat{\mathbf{P}}_f)$.

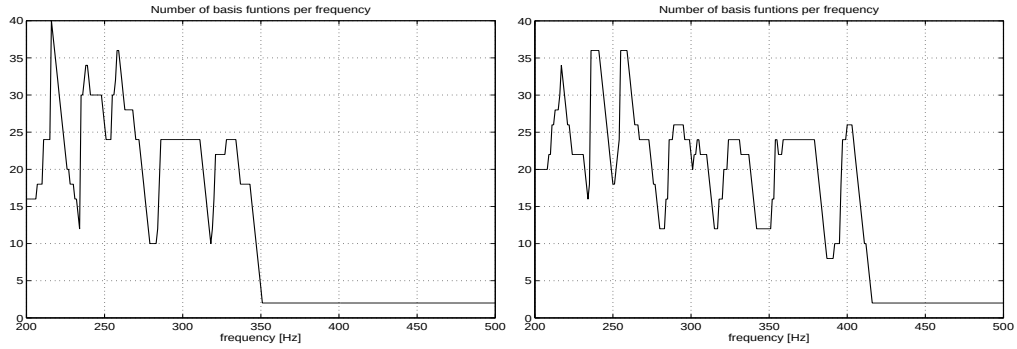

(a) (b)

Figure 5. Run 1: Number ℓ of POD ansatz functions over the frequency band $\mathcal{F}$ for $X = L_2(\Omega)$ (a) and for $X = H^1(\Omega)$ (b) with the tolerance $\varepsilon = 10^{-4}$ for the a-posteriori error estimator.

Compute the solutions $\hat{p}_f^\ell$ to (1) for $u = \hat{u}_f^\ell$ and $\hat{\lambda}_f^\ell$ to (2) for $p_f = \hat{p}_f^\ell$.
Set $\hat{\zeta}_f^\ell = \sigma(\hat{u}_f^\ell - u^\circ(f)) - \int_\Omega b(\mathbf{x})\hat{\lambda}_f^\ell(\mathbf{x})\,\mathrm{d}\mathbf{x}$.
if $|\hat{\zeta}_f^\ell| < \varepsilon$ **then**
Set flag $= 1$.
Return flag, ℓ, $\bar{u}_f^\ell$ and STOP.
else
Set $\ell = \ell + 2$.
end if
until $\ell > \ell^{\max}$
if flag $= 0$ **then**
Increase $\ell^{\max}$ and restart the algorithm.
break.
end if
end for

5. Numerical experiments

In this section, we present numerical experiments. One example is constructed in such a way that the optimal control is known. Thus, we can verify quality of the estimate (3). In the second example, the (exact) optimal control is unknown. All coding is done in MATLAB using routines from the PDE TOOLBOX with finite elements (FE). We apply a standard piecewise linear FE discretization with $m = 4957$ degrees of freedom.

Run 1: Let the impedance Z_f be given for the material melamine with $50mm$ depth; see Figure 1. We choose for the cost functional $\alpha = 0.1$, $\sigma = 1$ and

$$u_f^\circ = 10\bigg(\cos\Big(\frac{\pi(f-200)}{50}\Big) + \jmath\sin\Big(\frac{\pi(f-200)}{50}\Big)\bigg).$$

The measurement points $\mathbf{x}_i$, $i = 1, \ldots, n_\mathrm{m}$ with $n_\mathrm{m} = 12$ are depicted in Figure 2. The values p_f^i, $i = 1, \ldots, 12$, are given by $p_f^i = p_f(u_f^\circ)(\mathbf{x}_i)$, i.e., by the solution to (1) evaluated at $\mathbf{x}_i$ for $i = 1, \ldots, 12$ and $f \in \mathcal{F}$. Then, the optimal solution to $(\hat{\mathbf{P}}_f)$ is $u_f^* = u^\circ(f)$ for $f \in \mathcal{F}$. First we apply Algorithm **2** for the tolerance $\varepsilon = 10^{-4}$. In Figure 5, we present the number of ℓ of utilized POD basis functions for the choices $X = L_2(\Omega)$ and $X = H^1(\Omega)$. It turns out that the required tolerance is achieved

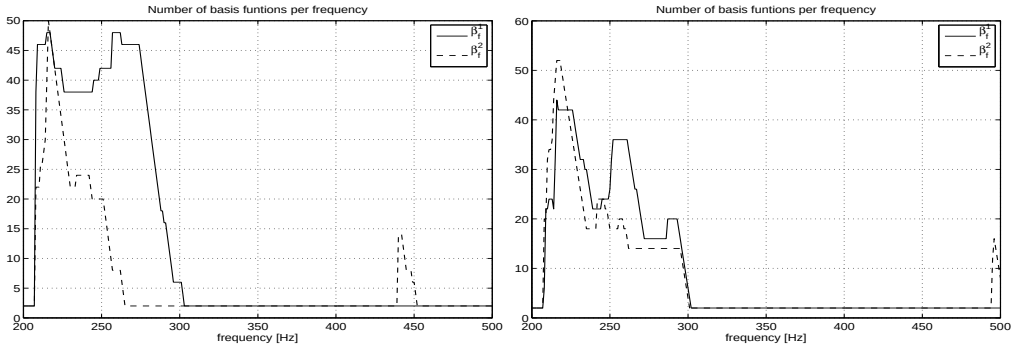

(a) (b)

Figure 6. Run 1: Number ℓ of RB ansatz functions over the frequency band $\mathcal{F}$ for $X = L_2(\Omega)$ (a) and for $X = H^1(\Omega)$ (b) with the tolerance $\varepsilon = 10^{-4}$ for the a-posteriori error estimator.

for all $f \in \mathcal{F}$ with $\ell \leq 40$ basis functions. We observe that the number of POD basis functions changes over the frequency band $\mathcal{F}$. Moreover, the different choices for X also influences the value of ℓ. The results for the reduced-basis method are given in Figure 6.

Compared to the POD approximations, the RB methods needs more basis functions at the beginning, but (significantly) less for $f \in (300, 350]$. The needed CPU times are presented in Table 1. Note, that for RBM Table 1 contains two columns, where the first one corresponds to $\hat{\beta}_f^1$ and the second one to $\hat{\beta}_f^2$ for approximating β_f.

Table 1. Run 1: CPU times in seconds.

Snapshot generation with FE	50.9	
POD computation	2.4	
POD optimization for $X = L_2(\Omega)$, $\varepsilon = 10^{-4}$	181.4	
POD optimization for $X = H^1(\Omega)$, $\varepsilon = 10^{-4}$	214.4	
POD optimization for $X = L_2(\Omega)$, $\varepsilon = 10^{-6}$	293.6	
POD optimization for $X = H^1(\Omega)$, $\varepsilon = 10^{-6}$	302.8	
Approximation of inf-sup constant	0.0	84.9
RBM computation	38.0	38.1
RBM optimization for $X = L_2(\Omega)$, $\varepsilon = 10^{-4}$	169.9	154.7
RBM optimization for $X = H^1(\Omega)$, $\varepsilon = 10^{-4}$	160.8	167.5
RBM optimization for $X = L_2(\Omega)$, $\varepsilon = 10^{-6}$	291.0	280.7
RBM optimization for $X = H^1(\Omega)$, $\varepsilon = 10^{-6}$	282.2	270.2

Next, we apply Algorithm **2** again with the smaller tolerance $\varepsilon = 10^{-6}$. In Figure 7, the number ℓ of utilized POD basis functions is plotted. The results for the reduced-basis method are given in Figure 8. Again, the required tolerance is achieved for all variants of the POD and RB method. As expected, more basis functions have to be included in our reduced-order modeling. Recall, that u_f^* denotes the optimal solution to $(\hat{\mathbf{P}}_f)$ and $\hat{u}_f^\ell \in \mathbb{C}$ denotes the suboptimal solution obtained from using ℓ basis functions. The decay of $\max_{f\in\Xi_f} |u_f^* - \hat{u}_f^\ell|$ is visualized in Figure 9 for $X = L_2(\Omega)$ using POD and RBM. Note, that we do not present the effectivity, i.e., the ratio between the true error $|u_f^* - \hat{u}_f^\ell|$ and its estimator $|\hat{\zeta}_f^\ell|/\sigma$, as it turns out to be bounded by 1.1 for all $f \in \Xi_f$.

Run 2: In the second example, we choose the same parameter as in the first run, but now $u_f^\circ = 0$. Thus, the optimal solution to $(\hat{\mathbf{P}}_f)$ is not known. We apply Algorithm **2** with the tolerance $\varepsilon = 10^{-6}$. In Figure 10, the number ℓ of utilized POD basis functions is plotted. The results for the reduced-basis method are given in Figure 11.

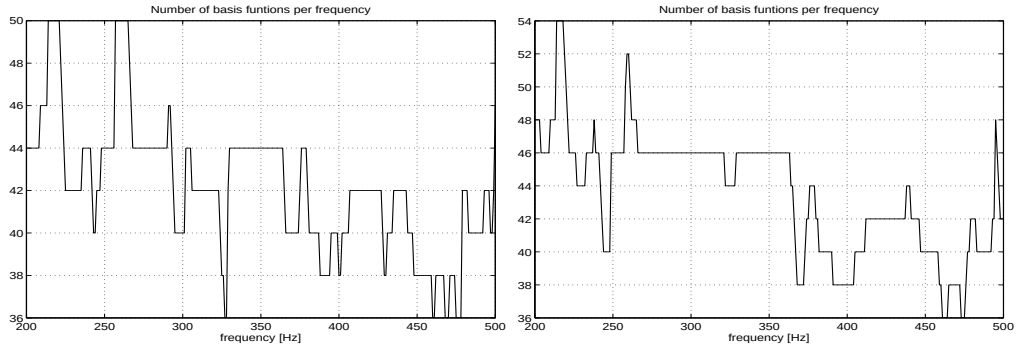

(a) (b)

Figure 7. Run 1: Number ℓ of POD ansatz functions over the frequency band $\mathcal{F}$ for $X = L_2(\Omega)$ (a) and for $X = H^1(\Omega)$ (b) with the tolerance $\varepsilon = 10^{-6}$ for the a-posteriori error estimator.

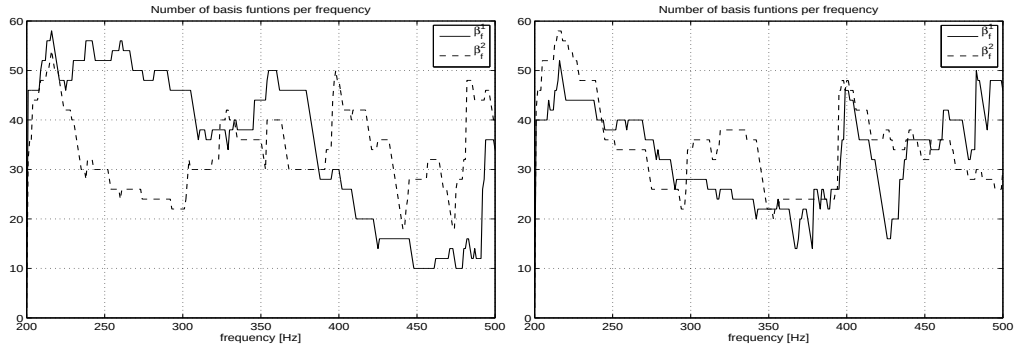

(a) (b)

Figure 8. Run 1: Number ℓ of RB ansatz functions over the frequency band $\mathcal{F}$ for $X = L_2(\Omega)$ (a) and for $X = H^1(\Omega)$ (b) with the tolerance $\varepsilon = 10^{-6}$ for the a-posteriori error estimator.

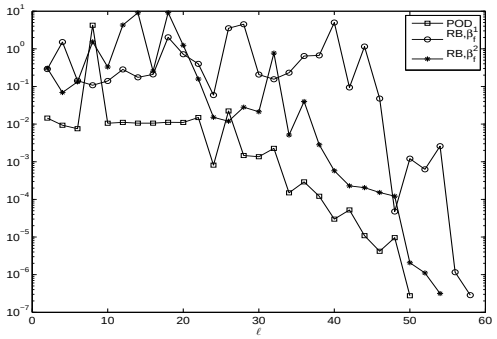

Figure 9. Run 1: Decay of $\max_{f\in\Xi_f} |u_f^* - \hat{u}_f^\ell|$ for POD and RBM in $X = L_2(\Omega)$.

6. Conclusion

We have compared RBM and POD for a linear-quadratic optimal control problem which is constrained by the Helmholtz equation. Thus, the following conclusions hold for this particular problem only. Moreover, it should be noted that the control $u \in \mathbb{C}$ (and thus the parameter for RBM and POD, respectively) is only formally two-dimensional (real and imaginary part) since we have seen that linear superposition allows to reduce the parameter dimension.

We have demonstrated that both methods are quite efficient, the differences are

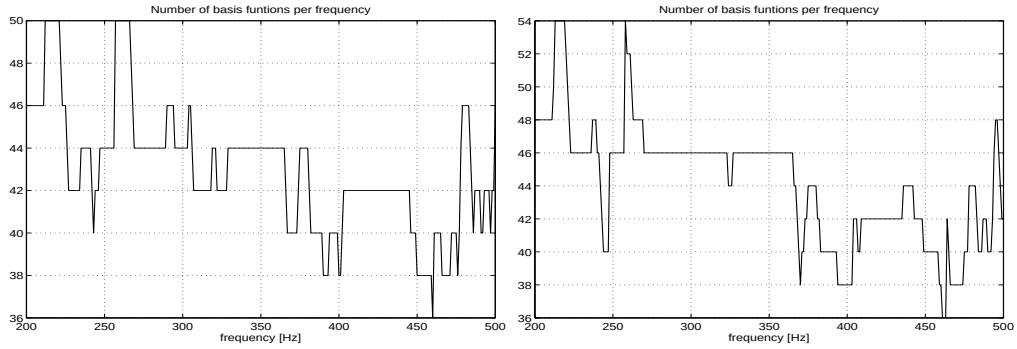

(a) (b)

Figure 10. Run 2: Number ℓ of POD ansatz functions over the frequency band $\mathcal{F}$ for $X = L_2(\Omega)$ (a) and for $X = H^1(\Omega)$ (b) with the tolerance $\varepsilon = 10^{-6}$ for the a-posteriori error estimator.

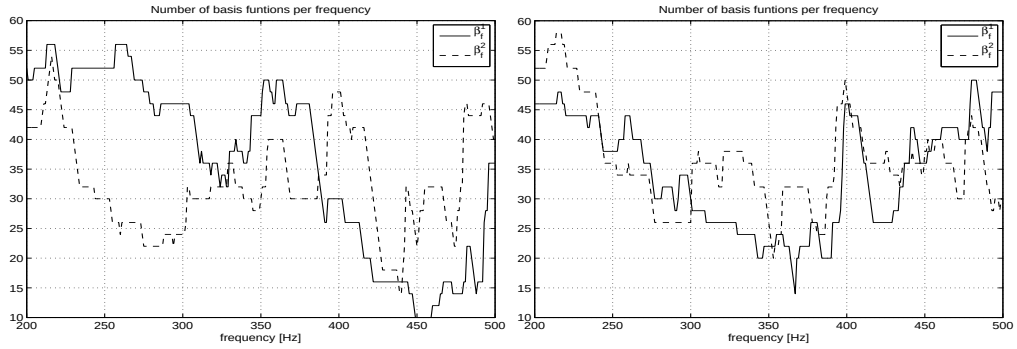

(a) (b)

Figure 11. Run 2: Number ℓ of RB ansatz functions over the frequency band $\mathcal{F}$ for $X = L_2(\Omega)$ (a) and for $X = H^1(\Omega)$ (b) with the tolerance $\varepsilon = 10^{-4}$ for the a-posteriori error estimator.

more or less marginal. As we can see in Table 1, RBM is a little more efficient than POD as long as we can avoid the computation of an approximation for the inf–sup constant. Also the average number of RBM modes is smaller than than the one for POD as we can deduce by the comparison of Figures 5,6 and Figures 7,8 for Run 1, Figures 10,11 for Run 2 as well as the CPU timings for Algorithm **2** in Table 1. On the other hand, Figure 9 shows that the true error in $L_2(\Omega)$ over the frequency sample Ξ_f is smaller for POD. This is somehow astonishing since the POD is known to be the best approximation of the state whereas here we consider the control. It also seems that POD earlier reaches the asymptotic regime.

Of course, these conclusions have to verified for different examples, in particular also for higher parameter dimensions.

References

[1] A.C. Antoulas *Approximation of Large-Scale Dynamical Systems (Advances in Design and Control) (Advances in Design and Control)*, Society for Industrial and Applied Mathematics, Philadelphia, PA, USA, 2005.

[2] P. Benner and E.S. Quintana-ortí, *Model reduction based on spectral projection methods*, in *Dimension Reduction of Large-Scale Systems* Springer-Verlag, 2005, pp. 5–45.

[3] S. Reed and B. Simon *Methods of Modern Mathematical Physics, I. Functional Analysis*, second Academic Press, San Diego, 1980.

[4] S. Volkwein, *Admittance identification from point-wise sound pressure measurements using reduced-order modelling*, (submitted 2009), .

[5] S. Volkwein and A. Hepberger, *Impedance identification by POD model reduction techniques*, at–Automatisierungstechnik 8 (2008), pp. 437–446.

[6] F. Tröltzsch and S. Volkwein, *POD a-posteriori error estimates for linear-quadratic optimal control problems*, Computational Optimization and Applications 44 (2009), pp. 83–115.

[7] M. Kahlbacher and S. Volkwein, *POD a-posteriori error based inexact SQP method for bilinear elliptic optimal control problems*, (submitted 2010), .

[8] P. Holmes, J. Lumley, and G. Berkooz *Turbulence, Coherent Structures, Dynamical Systems and Symmetry*, Cambridge University Press, Cambridge, 1996.

[9] K. Kunisch and S. Volkwein, *Galerkin Proper Orthogonal Decomposition Methods for a General Equation in Fluid Dynamics*, SIAM J. Numer. Anal. 40 (2002), pp. 492–515.

[10] N.C. Nguyen, *Reduced-Basis Approximations and A Posteriori Error Bounds for Nonaffine and Nonlinear Partial Differential Equations: Application to Inverse Analysis*, Singapore-MIT Alliance, 2005.

[11] D. Huynh, G. Rozza, S. Sen, and A. Patera, *A successive constraint linear optimization method for lower bounds of parametric coercivity and inf–sup stability constants*, Comptes Rendus Mathematique 345 (2007), pp. 473–478.